AGU PUBLICATIONS

Geophysical Research Letters

RESEARCH LETTER
10.1002/2014GL059579

Key Points:
- The hydraulic trap with higher TDS has been identified for the first time
- The continuous boundaries of local and regional flow systems have been mapped
- The magnetotelluric method is useful for large-scale flow system studies

Correspondence to:
X.-W. Jiang,
jxw@cugb.edu.cn

Citation:
Jiang, X.-W., L. Wan, J.-Z. Wang, B.-X. Yin, W.-X. Fu, and C.-H. Lin (2014), Field identification of groundwater flow systems and hydraulic traps in drainage basins using a geophysical method, *Geophys. Res. Lett.*, *41*, 2812–2819, doi:10.1002/2014GL059579.

Received 10 FEB 2014
Accepted 28 MAR 2014
Accepted article online 31 MAR 2014
Published online 16 APR 2014

Field identification of groundwater flow systems and hydraulic traps in drainage basins using a geophysical method

Xiao-Wei Jiang[1,2], Li Wan[1,2], Jun-Zhi Wang[1,2], Bin-Xi Yin[3], Wen-Xiang Fu[3], and Chang-Hong Lin[4]

[1]MOE Key Laboratory of Groundwater Circulation and Evolution, China University of Geosciences, Beijing, China, [2]School of Water Resources and Environment, China University of Geosciences, Beijing, China, [3]Ningxia Institute of Geological Survey, Yinchuan, China, [4]School of Geophysics and Information Technology, China University of Geosciences, Beijing, China

Abstract Groundwater flow systems and stagnant zones in drainage basins are critical to a series of geologic processes. Unfortunately, the difficulty of mapping flow system boundaries and no field example of detected stagnant zones restrict the application of the concept of nested flow systems. By assuming the variation in bulk resistivity of an aquifer with uniform porosity is mainly caused by groundwater salinity, the magnetotelluric technique is used to obtain the apparent resistivity of a profile across a groundwater-fed river in the Ordos Plateau, China. Based on the variations in apparent resistivity of the Cretaceous sandstone aquifer, the basin-bottom hydraulic trap below the river has been detected for the first time, and its size is found to be large enough for possible deposition of large ore bodies. The boundaries between local and regional flows have also been identified, which would be useful for groundwater exploration and calibration of large-scale groundwater models.

1. Introduction

As an important component of the hydrologic cycle and a crucial source of water supply, the mobilization and transport of chemical components are all linked to groundwater circulation [*Ingebritsen et al.*, 2006]. At the basin scale, the pattern of groundwater circulation has been found to be in the form of hierarchically nested flow systems, i.e., local, intermediate, and regional flow systems, as well as stagnation points among flow systems develop due to the periodic undulation of water table [*Tóth*, 1963], based on which the theory of regional groundwater flow [*Tóth*, 2009] develops. The existence of flow systems and/or stagnant zones (areas around stagnation points with low velocity) has been found to be critical to a series of geologic, biologic, and chemical processes (Figure 1)[*Batelaan et al.*, 2003; *Cardenas*, 2007; *Garven*, 1995; *Gleeson and Manning*, 2008; *Gomez and Wilson*, 2013; *Ingebritsen et al.*, 2006; *Marchetti and Carrillo-Rivera*, 2012; *Tóth*, 1980, 1999]. Stagnant zones can be classified as internal and basin-bottom ones [*Jiang et al.*, 2011]. Convergence of two flow systems results in an internal or a basin-bottom stagnant zone called hydraulic trap, where transported matter could accumulate [*Tóth*, 1980].

The spatial distribution of groundwater's effects is functionally related to the characteristic segments of flow systems [*Tóth*, 1999]. Therefore, mapping the spatial distribution of different flow systems is key to understand the geologic agency of groundwater. Identification of recharge and discharge zones based on topography and land surface features such as vegetation and soil [*Freeze and Cherry*, 1979; *Tóth*, 1966] is a practical way to get an initial impression of flow system distribution. However, the surface expressions resulting from nested flow systems do not carry information about the subsurface boundaries of flow systems. The hydrochemical trend based on a large amount of groundwater samples from representative wells is another good indicator to interpret the spatial distribution of flow systems [*Carrillo-Rivera et al.*, 2007; *Freeze and Cherry*, 1979; *Marchetti and Carrillo-Rivera*, 2012; *Tóth*, 1984, 1999]. However, mixing of groundwater from different depths of a well makes it difficult to map the boundaries of flow systems.

In sedimentary basins with no associated igneous rocks, the existence of most economically significant ore deposits is a result of the transport of solute by flowing groundwater [*Hough et al.*, 2008; *Ingebritsen et al.*, 2006]. Based on qualitative analysis, *Tóth* [1980, 1999] proposed that transported matter could accumulate in hydraulic traps. Studies by various researchers [*Baskov*, 1987; *Deming*, 1992; *Deming and Nunn*, 1991;

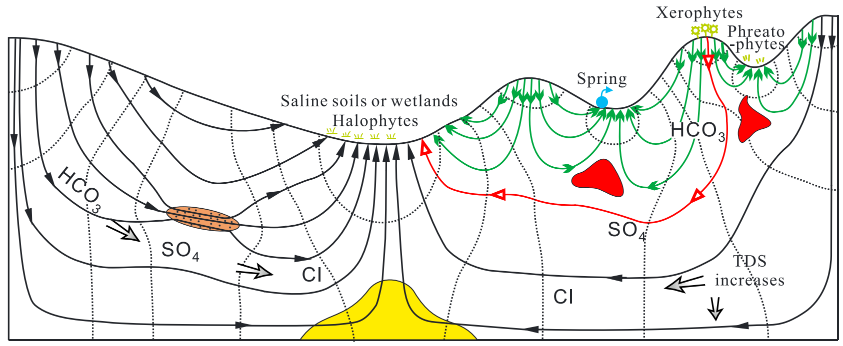

Figure 1. Schematic diagram showing some of the manifestations of the geologic agency of groundwater flow in drainage basins (modified from *Tóth*, 1999). The two red regions are internal hydraulic traps and the yellow region is a basin-bottom hydraulic trap. The green, red, and black flow lines represent local, intermediate, and regional flow systems, respectively.

Garven and Freeze, 1984; *Garven et al.*, 1993; *Person et al.*, 1996] show that the Mississippi Valley type ore deposits are the result of mobilization, transport, and accumulation of metal ions by groundwater, and the loci of accumulation and deposition are below the ancient groundwater discharge centers, which correspond to the basin-bottom hydraulic traps. Despite its importance, the hydraulic trap has not yet been physically detected in natural groundwater basins.

Groundwater chemistry and the chemical composition of rocks are dynamically coupled by the mineral-water equilibriums and by the rate and distance of groundwater circulation [*Ingebritsen et al.*, 2006]. Therefore, the residence time or age of groundwater [*Goode*, 1996] determines the type and rate of many geologic processes, including groundwater chemistry. In a drainage basin with uniform geology, due to the differences in residence time and travel distance, the salinity of groundwater (measured as total dissolved solids, TDS) in different flow systems could differ greatly. Generally, the regional and intermediate flow systems have much higher salinity than local flow systems. In the hydraulic traps, the accumulation of transported matter could lead to an even higher salinity [*Tóth*, 1980, 1999]. Moreover, evaporation could lead to salinization of shallow groundwater, which usually happens in discharge areas. The bulk resistivity of subsurface media, which can be measured by various geophysical methods, is highly dependent on the porosity, degree of saturation, and resistivity of groundwater [*Archie*, 1942]. Therefore, in a saturated aquifer with uniform porosity, the variation in bulk resistivity mainly caused by groundwater salinity provides an excellent indicator to distinguish the boundaries between local and regional flows, as well as the salinity anomaly in hydraulic traps and discharge areas.

The objective of this study is to test the application of magnetotelluric (MT) method for mapping resistivity differences, and identifying different flow systems and hydraulic traps. A large-scale profile across a groundwater-fed river is chosen as the study site.

2. Methods

The study site is located along a north-south trending cross section (NS) in the mid-lower reaches of the Dosit River Watershed in the Ordos Plateau, northwestern China (Figure 2a). According to the meteorological station at Otak, the mean annual precipitation is around 270 mm while the mean annual evaporation is around 2500 mm. The Dosit River, which develops at the lows of the watershed, originates near the city of Otak, and flows westward into the Yellow River, with a length of 166 km. The Dosit River is mainly supplied by groundwater discharge, with a trend of increasing TDS along the river.

In previous studies, the Cretaceous sandstone with sporadic clay lenses, which is poorly consolidated and high in porosity and permeability, has been considered as the main aquifer in the Ordos Plateau. The Jurassic sandstone, which is interbedded with thick clays and contains coals, is low in porosity and permeability. Because there is a layer of thick clay at the top of the Jurassic formation, the Jurassic formation has been considered to be the basement of the Ordos Plateau [*Hou et al.*, 2008a]. In the study site, the Cretaceous formation has a thickness of around 900–1000 m, and the Jurassic formation has a thickness of around 800–900 m.

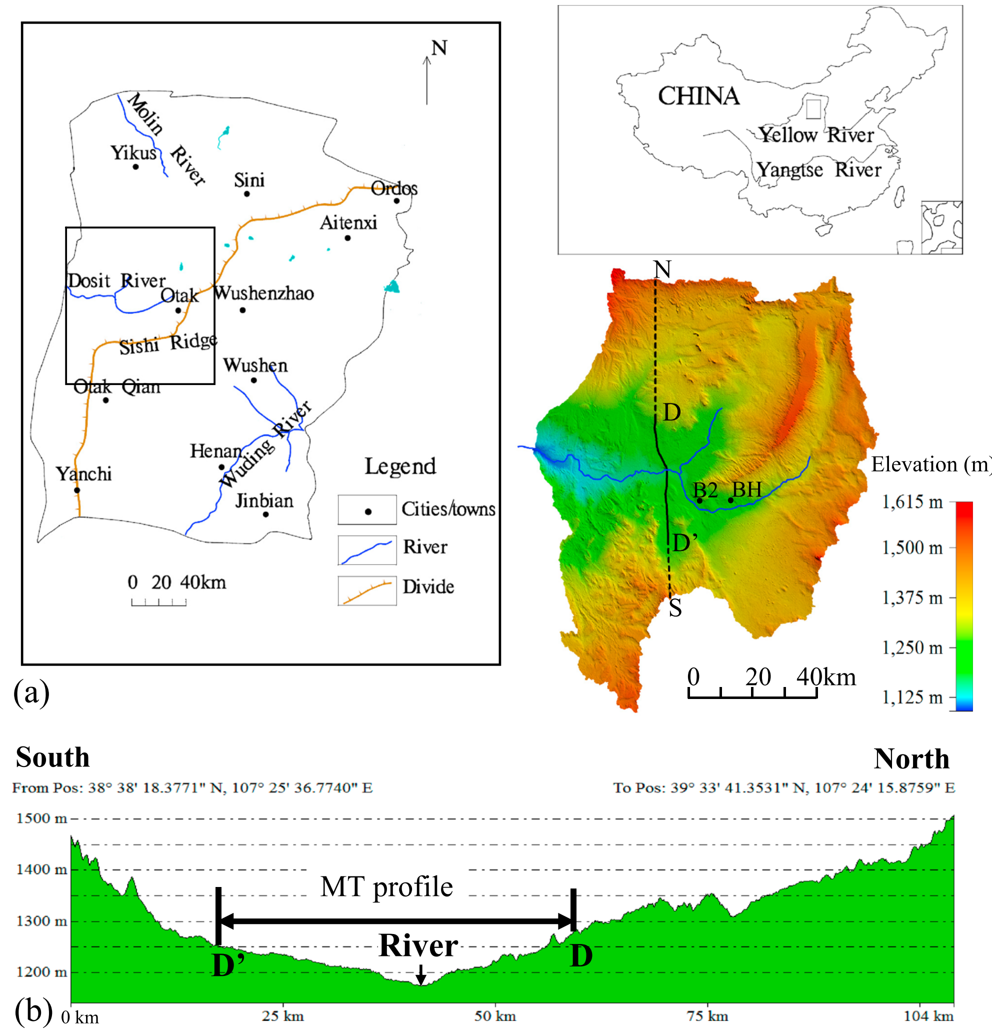

Figure 2. (a) Location and (b) topography of the study site. The N-S trending cross section is perpendicular to the Dosit River. The elevation differences between the divides and the river at the cross section are over 270 m.

The topography of the NS cross section is shown in Figure 2b. A series of previous studies reveal that groundwater flow is topography-driven because of the undulating topography, and the theory of regional groundwater flow is applicable to Cretaceous aquifer in the Ordos Plateau [*Hou et al.*, 2008b; *Jiang et al.*, 2012; *Yin et al.*, 2010]. Based on the numerical results that there is an abrupt change in groundwater age at the system boundary in the middle and lower reaches of a drainage basin [*Gomez and Wilson*, 2013; *Jiang et al.*, 2010; *Jiang et al.*, 2012] and the assumption that an older age would lead to a higher salinity, MT measurements were carried out only at the middle part of the NS section, denoted as DD′.

In recent years, the spatial distribution of electrical resistivity obtained using electrical or electromagnetic geophysical surveys has been successfully used in hydrological studies to differentiate different sources of water based on salinity differences in the subsurface [*Bauer et al.*, 2006; *Befus et al.*, 2012; *Cardenas and Markowski*, 2011; *Day-Lewis et al.*, 2006; *Ong et al.*, 2010; *Van Dam et al.*, 2009]. However, all of these studies are limited to small scales both horizontally and vertically. Here the MT method is chosen because of its great penetration depth, which can be as deep as hundreds of kilometers. The MT (including audiofrequency MT, denoted as AMT, and controlled-source audiofrequency MT, denoted as CSAMT) method has been successfully applied in such activities as exploration of mineral resources and hydrocarbon, identification of seawater intrusion and groundwater pollution, and mapping of weak zones during geotechnical investigations [*Reynolds*, 2011].

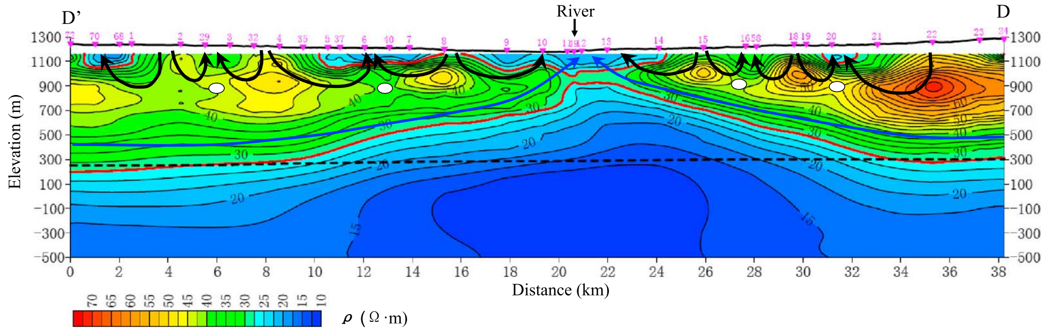

Figure 3. Distribution of apparent resistivity and schematic streamlines along profile DD′. The pink numbers and triangles are locations of the MT measurements, the black solid lines are contour of resistivity, the black dashed line is the boundary of the Cretaceous and Jurassic formations, the black solid bold lines with arrows are streamlines of local flow systems, the blue solid lines with arrows are streamlines of regional flow systems, and the white circles are internal hydraulic traps.

In the study site, although variations in TDS inside the Cretaceous sandstone is what we mainly care about, to ensure convincing results, the TDS in the shallow part of the Jurassic sandstone should also be measured. Therefore, the penetration depth should be at least 1.5 km. The instrument used is the STRATAGEM EH4 equipped with low-frequency optional receiver (0.1 Hz to 1000 Hz)[*Geometrics*, 2000]. Electrical resistivity information is calculated from measurements of surface electric and magnetic fields along the profile. At each measurement site, the magnetic fields are detected with two perpendicular H-field sensors, and the electric fields are detected by measuring the differential voltage between the two electrodes of the electric dipole. Because an MT sounding provides an estimate of vertical resistivity beneath the receiver site, electrical resistivity at different depths can be obtained by measuring signals over a wide frequency range. Higher-frequency data are influenced by shallow or nearby features, and lower frequency data are influenced by structures at greater depth.

The spacing of MT measurements was initially set to be 2000 m. At some locations, the spacing is reduced to be around 500 m. Data collection and analysis are processed using the IMAGEM program distributed with the STRATAGEM EH4 [*Geometrics*, 2000]. The 1-D analysis is based on the Bostick transformation. The apparent resistivity is calculated from the ratio of the amplitudes of the magnetic and electrics fields generated by currents in the ground, which can be written as

$$\rho = \frac{1}{5f}\left|\frac{E}{H}\right|^2 \tag{1}$$

where ρ is apparent resistivity, f is frequency of signal, E is amplitude of the electric field, and H is amplitude of the orthogonal magnetic field. The skin depth, δ, which is determined by the apparent resistivity and frequency, is calculated by

$$\delta = 500\sqrt{\frac{\rho}{f}} \tag{2}$$

Using equation (2), the relationship between apparent resistivity and depth can be established. If ρ equals 10 $\Omega \cdot$m, the frequency 1000 Hz corresponds to a depth of 50 m and the frequency 1 Hz corresponds to a depth of 1581 m. If ρ equals 50 $\Omega \cdot$m, the frequency 1000 Hz corresponds to a depth of 112 m and the frequency 5 Hz corresponds to a depth of 1581 m. Therefore, the available signals cannot provide resistivity information of the shallow subsurface, which is a limitation of the instrument, but is enough to obtain information of the whole Cretaceous formation and most part of the Jurassic formation. After removal of noisy data, a 2-dimensional image of apparent resistivity can be obtained by using the 2-D analysis function of IMAGEM.

3. Results

Figure 3 shows the apparent resistivity ranges between 10 and 72 $\Omega \cdot$m, which is consistent with reported electrical resistivity observations in Mesozoic terrestrial sedimentary rocks [*Keller and Frischknecht*, 1966, Table 10]. The black dashed line is the boundary between the Jurassic and Cretaceous formations inferred from nearby borehole data [*Hou et al.*, 2008a]. Generally, the apparent resistivity in the Jurassic formation is low and in the Cretaceous formation is high. Although there are no wells deeper than 200 m

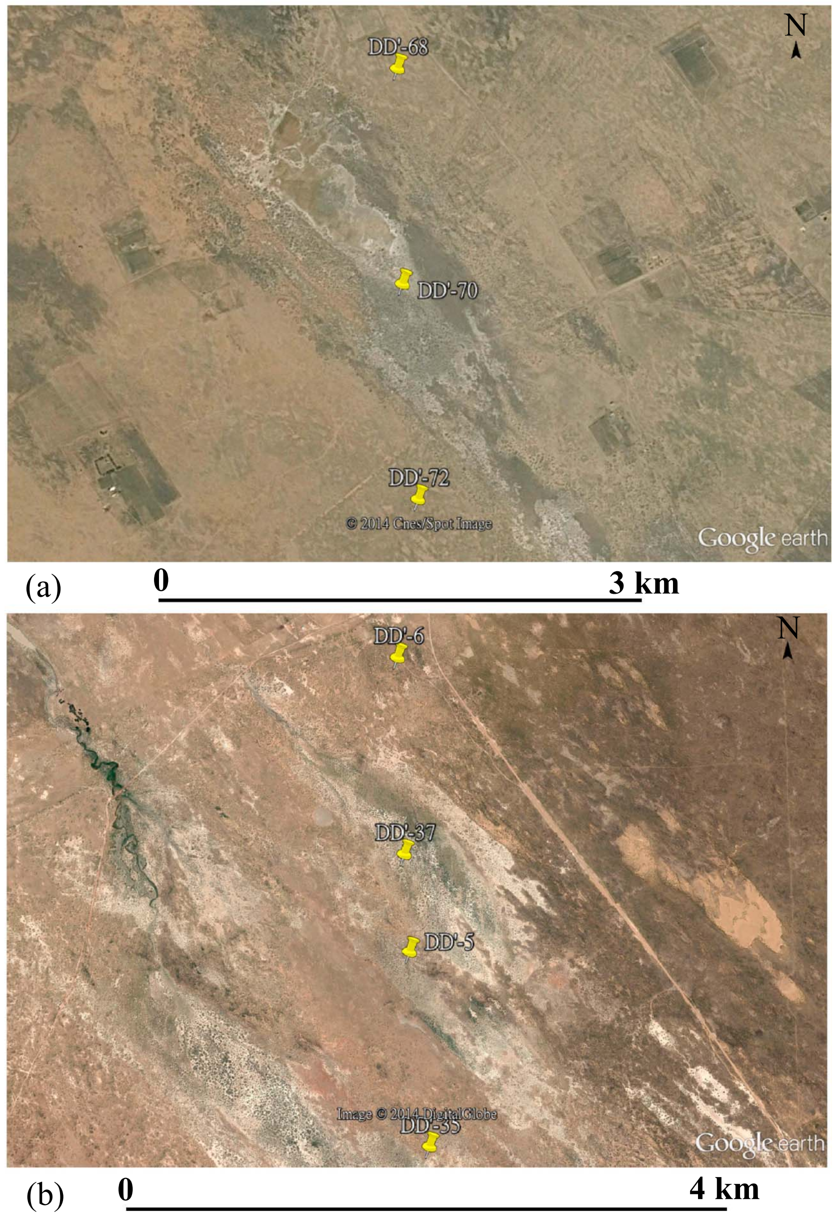

Figure 4. Google Earth images of saline-alkali soils in discharge areas. The yellow labels represent locations of MT measurements. The regions around measurement sites 70, 37, and 5 are saline-alkali soils.

along the profile, there are numerous deep wells in the upper and middle reaches of the watershed near the river, whose hydrogeologic conditions are generally the same as that of the profile. The TDS of well BH with a depth of 1400 m, which taps the Jurassic sandstone, is as high as 8499 mg/L. However, the TDSs of all the deep wells ($>$ 150 m) near the well BH, which tap the Cretaceous sandstone, are all below 1000 mg/L. Although the apparent resistivity difference in the two formations might also be influenced by the porosity structure, it is consistent with the drastic difference in TDS of groundwater from the two formations.

Inside the Jurassic and Cretaceous formations, even at the same depth or elevation, there are also significant variations in apparent resistivity. For the Jurassic formation and the deep part of the Cretaceous formation, in the regions away from the river, the contour of apparent resistivity equaling 27.5 $\Omega \cdot$m corresponds to the boundary of formations, and the contour lines are almost horizontal; however, near the river, the contour lines are no longer horizontal, instead, they have an upward trend. Due to the relatively uniform porosity structure inside the Cretaceous formations in the Ordos Plateau [*Hou et al*., 2008a], this phenomenon implies a higher TDS of groundwater in the deep part of the basin below the river. Such a phenomenon has also been supported by a borehole near the Dosit River, which is only 8 km away from the profile. In borehole B2, groundwater was sampled from three sections of the Cretaceous aquifer. From the shallow to the deep, the TDS were measured to be 580, 514, and 930 mg/L, respectively.

According to the topography of the NS cross section, we can infer that there are two regional flow systems, one originates from the highs near the north divide and the other from the south divide, and both of them discharge to the Dosit River. The two regional flow systems meet at the basin bottom below the river (Figure 3). Therefore, the zone with lower apparent resistivity in the deep part of the basin below the river can be interpreted as the basin-bottom hydraulic trap due to convergence of two flow systems. Here the horizontal extent of the hydraulic trap (the zone where resistivity contours have an upward trend) is over 20 km, which is about 1/5 of the length of the NS cross section. The large size of the hydraulic trap reveals that it is an ideal place for ore deposition, and the size of the expected ore body could be large enough.

Although apparent resistivity data are missing near the ground surface, in the shallow part around 100 m below surface, there are also areas with lower electrical resistivity, which correspond to lower elevation at the ground surface, i.e., discharge areas. The discharge areas with apparent resistivity below $27.5\Omega\cdot m$ have been successfully correlated to surface features along the profile. Surface water sampled at the Dosit River has a TDS of 2037 mg/L, which is higher than TDS of groundwater from nearby wells with depths ranging between 200 m and 350 m. The two discharge areas near measurement sites 70 and 5 are saline-alkali soils (Figure 4). The discharge area near measurement site 20 corresponds to an ancient river channel.

In the vertically middle part of the Cretaceous formation, there are also variations in apparent resistivity. The red or yellow areas with higher electrical resistivity correspond to relatively higher elevation at the ground surface, i.e., recharge areas. The flow paths from local highs of topography to adjacent local lows constitute local flow systems (Figure 3). The areas with relatively lower electrical resistivity, which locate between the red or yellow areas and below the local lows, can be interpreted as the internal hydraulic traps. Because an internal stagnation point separate four flow systems [*Anderson and Munter*, 1981; *Jiang et al*., 2011], the internal hydraulic traps can be used to determine the boundaries between local flow and regional flow.

It is important to note that the observed resistivity data inside the Cretaceous formation are unlikely to be explained by textural heterogeneity caused by the sporadic clays. The thin clay lenses, whose thickness rarely exceed several meters, hardly influence the resistivity data because the larger penetration depth of the MT method is sacrificed by lower resolution. Based on the analysis above, the resistivity anomalies inside the Cretaceous formation are most likely attributed to variations in groundwater salinity.

4. Conclusions

MT measurements were conducted along a profile across the Dosit River, where the assumption of 2-D groundwater flow is suitable. Based on the fact that the aquifer has a uniform porosity structure, the apparent bulk resistivity is used to represent the variation in groundwater salinity. Although the apparent resistivity in the Jurassic formation is also influenced by the upward groundwater flow below the river, we mainly analyze the variation in apparent resistivity in the Cretaceous aquifer. It is shown that there is a hydraulic trap at the deep part of the Cretaceous formation with lower apparent resistivity, i.e., with higher TDS. This phenomenon has been verified by groundwater sampled from different depths of a nearby borehole. This is the first time that the dimension of a basin-bottom hydraulic trap has been demonstrated in a real basin. The existence of hydraulic traps (or stagnant zones) confirms that transported matter could accumulate and deposit below regional discharge centers, and the large size of the basin-bottom stagnant zone indicates that the size of ore bodies below regional discharge centers could be large. This has great implications on the mechanism of ore deposition.

Based on the variations in apparent resistivity in the shallow and middle parts of the Cretaceous formation, the local flow systems and internal hydraulic traps, and thus the boundaries between local flow and regional flow, can also be identified. These continuous boundaries could be useful to exploring drinkable groundwater in arid and semiarid regions and could be an important indicator for calibrating regional scale groundwater flow and solute transport models.

Although only one example application is presented here, the technique can be used in other basin scale studies. Exploring the 3-D characteristics of hydraulic traps (or stagnant zones) and boundaries of flow systems in field basins is an important area for future research.

Acknowledgments
This study is supported by the China Geological Survey (1212011121145), the Program for New Century Excellent Talents in Universities (NCET-13-1007), and partially by the Beijing Higher Education Young Elite Teacher Project (YETP0656), Research Fund for the Doctoral Program of Higher Education of China (20120022120001), and the Fundamental Research Funds for the Central Universities of China. The raw data of the magnetotelluric measurements are available from the author upon request.

The Editor thanks two anonymous reviewers for their assistance in evaluating this paper.

References

Anderson, M. P., and J. A. Munter (1981), Seasonal reversals of groundwater flow around lakes and the relevance to stagnation points and lake budget, *Water Resour. Res.*, *17*, 1139–1150, doi:10.1029/WR017i004p01139.

Archie, G. E. (1942), The electrical resistivity log as an aid in determining some reservoir characteristics, *Pet. Trans. AIME*, *146*, 54–62.

Baskov, E. A. (1987), *The Fundamentals of Paleohydogeology of Ore Deposits*, Springer-Verlag, Berlin.

Batelaan, O., F. De Smedt, and L. Triest (2003), Regional groundwater discharge: Phreatophyte mapping, groundwater modelling and impact analysis of land-use change, *J. Hydrol.*, *275*(1), 86–108, doi:10.1016/S0022-1694(03)00018-0.

Bauer, P., R. Supper, S. Zimmermann, and W. Kinzelbach (2006), Geoelectrical imaging of groundwater salinization in the Okavango Delta, Botswana, *J. Appl. Geophys.*, *60*(2), 126–141, doi:10.1016/j.jappgeo.2006.01.003.

Befus, K., M. B. Cardenas, J. Ong, and V. Zlotnik (2012), Classification and delineation of groundwater–lake interactions in the Nebraska Sand Hills (USA) using electrical resistivity patterns, *Hydrogeol. J.*, *20*(8), 1483–1495, doi:10.1007/s10040-012-0891-x.

Cardenas, M. B. (2007), Potential contribution of topography-driven regional groundwater flow to fractal stream chemistry: Residence time distribution analysis of Tóth flow, *Geophys. Res. Lett.*, *34*, L05403, doi:10.1029/2006GL029126.

Cardenas, M. B., and M. S. Markowski (2011), Geoelectrical imaging of hyporheic exchange and mixing of river water and groundwater in a large regulated river, *Environ. Sci. Technol.*, *45*(4), 1407–1411, doi:10.1021/es103438a.

Carrillo-Rivera, J. J., I. Varsányi, L. Kovács, and A. Cardona (2007), Tracing groundwater flow systems with hydrogeochemistry in contrasting geological environments, *Water Air Soil Pollut.*, *184*(1–4), 77–103, doi:10.1007/s11270-007-9400-6.

Day-Lewis, F., E. White, C. Johnson, J. Lane Jr., and M. Belaval (2006), Continuous resistivity profiling to delineate submarine groundwater discharge—Examples and limitations, *The Leading Edge*, *25*(6), 724–728, doi:10.1190/1.2210056.

Deming, D. (1992), Catastrophic release of heat and fluid flow in the continental crust, *Geology*, *20*(1), 83–86, doi:10.1130/0091-7613(1992)020<0083:crohaf>2.3.co;2.

Deming, D., and J. A. Nunn (1991), Numerical simulations of brine migration by topographically driven recharge, *J. Geophys. Res.*, *96*(B2), 2485–2499, doi:10.1029/90jb02392.

Freeze, R. A., and J. A. Cherry (1979), *Groundwater*, Prentice-Hall, Inc., Englewood Cliffs, N. J.

Garven, G. (1995), Continental-scale groundwater-flow and geologic processes, *Annu. Rev. Earth Planet. Sci.*, *23*, 89–117, doi:10.1146/annurev.ea.23.050195.000513.

Garven, G., and R. A. Freeze (1984), Theoretical analysis of the role of groundwater-flow in the genesis of stratabound ore-deposits .1. Mathematical and numerical model, *Am. J. Sci.*, *284*(10), 1085–1124, doi:10.2475/ajs.284.10.1085.

Garven, G., S. Ge, M. A. Person, and D. A. Sverjensky (1993), Genesis of stratabound ore deposits in the midcontinent basins of North America. 1. The role of regional groundwater flow, *Am. J. Sci.*, *293*, 497–568.

Geometrics, I. (2000), Operation manual for Stratagem systems running IMAGEM (Ver. 2.16), Rep., 1–38 pp., San Jose, Calif.

Gleeson, T., and A. H. Manning (2008), Regional groundwater flow in mountainous terrain: Three-dimensional simulations of topographic and hydrogeologic controls, *Water Resour. Res.*, *44*, W10403, doi:10.1029/2008WR006848.

Gomez, J. D., and J. L. Wilson (2013), Age distributions and dynamically changing hydrologic systems: Exploring topography-driven flow, *Water Resour. Res.*, *49*, 1503–1522, doi:10.1002/wrcr.20127.

Goode, D. J. (1996), Direct simulation of groundwater age, *Water Resour. Res.*, *32*, 289–296, doi:10.1029/95WR03401.

Hou, G. C., M. S. Zhang, F. Liu, Y. H. Wang, Y. P. Liang, and Z. P. Tao (2008a), *Groundwater Investigation in the Ordos Basin* [in Chinese], Geological Publishing House, Beijing, China.

Hou, G. C., Y. P. Liang, X. S. Su, Z. H. Zhao, Z. P. Tao, L. H. Yin, Y. C. Yang, and X. Y. Wang (2008b), Groundwater systems and resources in the Ordos Basin, China, *Acta Geol. Sin.-Engl. Ed.*, *82*(5), 1061–1069, doi:10.1111/j.1755-6724.2008.tb00664.x.

Hough, R. M., et al. (2008), Naturally occurring gold nanoparticles and nanoplates, *Geology*, *36*(7), 571–574, doi:10.1130/g24749a.1.

Ingebritsen, S. E., W. E. Sanford, and C. E. Neuzil (2006), *Groundwater in Geological Processes*, 2nd ed., Cambridge Univ. Press, Cambridge, U. K.

Jiang, X. W., X. S. Wang, L. Wan, and S. Ge (2011), An analytical study on stagnant points in nested flow systems in basins with depth-decaying hydraulic conductivity, *Water Resour. Res.*, *47*, W01512, doi:10.1029/2010WR009346.

Jiang, X. W., L. Wan, M. B. Cardenas, S. Ge, and X. S. Wang (2010), Simultaneous rejuvenation and aging of groundwater in basins due to depth-decaying hydraulic conductivity and porosity, *Geophys. Res. Lett.*, *37*, L05403, doi:10.1029/2010GL042387.

Jiang, X. W., L. Wan, S. Ge, G.-L. Cao, G.-C. Hou, F.-S. Hu, X.-S. Wang, H. Li, and S.-H. Liang (2012), A quantitative study on accumulation of age mass around stagnation points in nested flow systems, *Water Resour. Res.*, *48*, W12502, doi:10.1029/2012wr012509.

Keller, G. V., and F. C. Frischknecht (1966), *Electrical Methods in Geophysical Prospecting*, Pergamon Press, New York.

Marchetti, Z. Y., and J. J. Carrillo-Rivera (2012), Tracing groundwater discharge in the floodplain of the Parana River, Argentina: Implications for its biological communities, *River Res. Applic.*, *30*, 166–179, doi:10.1002/rra.2629.

Ong, J., J. Lane Jr., V. Zlotnik, T. Halihan, and E. White (2010), Combined use of frequency-domain electromagnetic and electrical resistivity surveys to delineate near-lake groundwater flow in the semi-arid Nebraska Sand Hills, U.S.A., *Hydrogeol. J.*, *18*(6), 1539–1545, doi:10.1007/s10040-010-0617-x.

Person, M., J. P. Raffensperger, S. Ge, and G. Garven (1996), Basin-scale hydrogeologic modeling, *Rev. Geophys.*, *34*(1), 61–87, doi:10.1029/95rg03286.

Reynolds, J. M. (2011), *An Introduction to Applied and Environmental Geophysics*, 2nd ed., Wiley-Blackwell, Oxford, U. K.

Tóth, J. (1963), A theoretical analysis of groundwater flow in small drainage basins, *J. Geophys. Res.*, *68*, 4795–4812, doi:10.1029/JZ068i008p02354.

Tóth, J. (1966), Mapping and interpretation of field phenomena for groundwater reconnaissance in a prairie environment, Alberta, Canada, *Int. Assoc. Sci. Hydrol. Bull.*, *9*(2), 20–68.

Tóth, J. (1980), Cross-formational gravity-flow of groundwater: A mechanism of the transport and accumulation of petroleum (The generalized hydraulic theory of petroleum migration), in *Problems of Petroleum Migration*, edited by W. H. I. Roberts and R. J. Cordell, pp. 121–167, The American Association of Petroleum Geologists, Tulsa, Okla.

Tóth, J. (1984), The role of regional gravity flow in the chemical and thermal evolution of groundwater, paper presented at Proceedings of First Canadian/American Conference on Hydrogeology, National Water Well Association, Worthington, Ohio, U.S.A., Banff, Alberta, Canada.

Tóth, J. (1999), Groundwater as a geologic agent: An overview of the causes, processes, and manifestations, *Hydrogeol. J.*, *7*(1), 1–14, doi:10.1007/s100400050176.

Tóth, J. (2009), *Gravitational Systems of Groundwater Flow: Theory, Evaluation and Utilization*, Cambridge Univ. Press, Cambridge, U. K.

Van Dam, R. L., C. T. Simmons, D. W. Hyndman, and W. W. Wood (2009), Natural free convection in porous media: First field documentation in groundwater, *Geophys. Res. Lett.*, *36*, L11403, doi:10.1029/2008gl036906.

Yin, L. H., G. C. Hou, Z. P. Tao, and Y. Li (2010), Origin and recharge estimates of groundwater in the Ordos Plateau, People's Republic of China, *Environ Earth Sci.*, *60*, 1731–1738, doi:10.1007/s12665-009-0310-3.